A NOVEL MECHANISM OF HUMAN PLASTIN REGULATION

Christopher L. Schwebach[1]

INTRODUCTION

The actin cytoskeleton drives numerous important cellular processes including migration, cytokinesis, and endo- and exocytosis[1,2]. Coordination of these processes requires precise regulation of actin dynamics, localization, and superstructure. This regulation is achieved by over 150 actin-binding proteins integrating various signals[3]. Among these proteins are actin-bundling proteins that non-covalently crosslink actin filaments into meshes and bundles[3]. Plastins, also known as fimbrins, are one family of actin-bundling proteins conserved throughout eukaryotic life[4,5].

Vertebrates express three tissue-specific plastin isoforms. Plastin1 (PLS1, I-plastin) is primarily expressed in the intestines and kidneys contributing to the microvilli in the epithelial brush border[6,7]. It is also expressed in the hair cells of the inner ear contributing to the actin-based stereocilia[8,9]. Plastin2 (PLS2, L-plastin) is expressed in hematopoietic cells contributing to immune cell migration, invasion, and activation[10-16]. Intriguingly, PLS2 is ectopically expressed in ~70% of epithelial cancers and has been shown to contribute to their metastatic capabilities[17-21]. Plastin3 (PLS3, T-plastin) is ubiquitously expressed in solid tissues where it's role is not well understood[17].

Plastins bundle actin through two tandem actin-binding domains (ABD1 and ABD2). Each of these binds an individual filament bringing them together into a tight bundle[22,23]. Preceding the actin-binding core is an N-terminal regulatory headpiece (Hp) domain containing two Ca^{2+}-binding EF-hand motifs. Upon Ca^{2+} binding the ability of plastins to bundle is diminished[7,24,25].

[1] Other contributors to this work: Jonathan C. Wright, Elena Kudryashova and Dmitri S. Kudryashov

Beyond the role of Ca^{2+} in the regulation of actin bundling by plastins, very little is understood concerning the molecular mechanisms underpinning the various cellular functions of the plastin isoforms.

Previous work has shown that the actin-binding domains are not identical. Electron microscopy analysis of 2D actin arrays suggested that binding of plastin to an actin filament through one ABD determined how the subsequent ABD would bundle the adjacent filament[23]. The structure of ABD2 bound to F-actin was elucidated by cryo-electron microscopy, however, reconstruction of ABD1 bound to the filament was not achieved likely due to multiple binding modes[26]. Intriguingly, our recent work has demonstrated that ABD1 is the primary actin-binding domain that binds to the filament both in the absence and presence of Ca^{2+}, whereas ABD2 is only associated with filaments upon bundling[27]. Taken together these studies demonstrate a distinct difference in the properties of the ABDs. To date, no study has thoroughly investigated the differences and regulation of the individual ABDs.

In this study, we addressed these gaps in our understanding using various biochemical techniques to characterize the ABDs of PLS2 and described a novel mechanism of plastin regulation. We found that ABD2 possesses unique properties not observed in a full-length context. ABD2 binds F-actin with over 300-fold higher affinity than either ABD1 or full-length PLS2. ABD2 is also unique in its ability to nucleate actin filaments. This nucleation ability is inhibited when ABD1 is introduced *in trans*. We re-examined previously described plastin mutations which suggest that disruption of the ABD1-2 interface releases ABD1's inhibition of ABD2. Finally, we show that this inhibition can be released in a physiological context through ABD1 binding F-actin.

RESULTS

The affinity of PLS2 ABD2 for F-actin is much higher than the affinity of full-length PLS2.

We have previously shown that PLS3 ABD1 binds actin with an affinity similar to that of full-length PLS3[27]. Using high-speed (>300,000 xg) co-sedimentation assays we found that PLS2 ABD1 binds with micromolar affinity (1.29 ± 0.39 μM) comparable to that of full-length PLS2 (5.66 ± 0.96 μM) (Fig. 1a, d). Interestingly, the same co-sedimentation experiments revealed that PLS2 ABD2 binds F-actin with a much higher affinity than either ABD1 or full-length, however, we could not accurately assess K_d's for ABD2 using this due to a poor applicability of this method for measuring low quantities of interacting proteins. Using fluorescence anisotropy (FA) we found that fluorescein-labeled ABD2 (FM-ABD2) binds F-actin with nanomolar affinity (30.99 ± 5.46 nM), i.e. over 150-fold stronger than either ABD1 or full-length PLS2 (Fig. 1b, d). To confirm that the high affinity was not due to the fluorescein modification, we determined the affinity of unlabeled ABD2 in a FA competition assay. F-actin and FM-ABD2 were added at saturating concentrations and unlabeled ABD2 was titrated to observe the dissociation of FM-ABD2 from actin. Unlabeled ABD2 bound actin with an affinity in low nanomolar range (4.14 ± 0.89 nM; Fig. 1c, d), more than 300 times stronger than ABD1 or full-length PLS2.

PLS2 ABD2 nucleates actin filaments and is inhibited by ABD1

Previous work has shown that ABD2 from *Schizosaccharomyces pombe* Fim1 can nucleate actin filament growth[28]. We tested if this is also true for PLS2 ABD2 using bulk pyrene-actin polymerization assays. ABD2 potently increased actin filament assembly even at low nanomolar concentrations (Fig. 2a). To confirm that this observation is due to nucleation, we observed polymerization of individual filaments using total internal fluorescence microscopy (TIRFm). ABD2 significantly increased the number of filaments as compared to actin alone (Fig. 2b).

It is curious that the observed potent nucleating ability has not seen in the full-length plastin context. This suggests suppression of ABD2's nucleation in a full protein context. To test this hypothesis, we added ABD1 *in trans* to pyrene assays containing 2.5 µM actin and 250 nM ABD2. ABD1 inhibited ABD2's nucleating ability in a dose-dependent manner (Fig. 2c) suggesting ABD1 suppression of ABD2.

PLS2 ABD1 and ABD2 interact in *trans* with nanomolar affinity.

To further understand the interaction between ABD1 and ABD2 we determined their affinity for each other. Using FA we found that PLS2 ABD1 binds FM-ABD2 with a high affinity (20.53 ± 2.17 nM; Fig. 2a, m). Addition of the regulatory headpiece (Hp) slightly decreased the affinity independent of Ca^{2+} binding (EGTA: 29.83 ± 3.77 nM, Ca^{2+}: 30.75 ± 3.28 nM; Fig. 3d, m). The affinity of PLS2 ABD1 for unlabeled ABD2 was 2 – 10 -fold higher as determined by the FA competition assay (Fig. 3b, e, m). Similarly, PLS2 ABD2 was able to bind PLS3 ABD1, however, the presence of Hp domain substatnially increased, rather than decreased the affinity of the construct to FM-ABD2 (Fig. 3g, h, j, k, m).

Protein-protein interactions commonly increase the stability of the proteins, which can be detected by protein melting experiments. We tested whether *in trans* ABD binding stabilized the domains using differential scanning fluorimetry (DSF). In all cases, the presence of both ABDs increased the melting temperature by 1 to 5 °C, however, they remained less stable than full-length PLS2 or the PLS2 actin-binding core lacking the Hp (Fig. 3c, f, i, l and Fig. 4).

Mutations in ABD1 release inhibition of ABD2 by ABD1

Early research in *Saccharomyces cerevisiae* identified nine mutations in ABD1 of yeast plastin (Sac6) that rescued defects of a mutant actin phenotype[29]. It was hypothesized that these mutations were on the actin-binding interface and increased plastin-actin binding. Since this study,

the crystal structures of *S. pombe* and *Arabidopsis thaliana* plastin cores have been solved[23]. The investigation revealed that the identified residues are not surface-exposed and several are buried in the ABD1-2 interface. We hypothesized that the rescuing activity of the Sac6 mutants could stem from the release of the ABD1 suppression of ABD2. We generated several homologous PLS2 mutants using multi-site directed mutagenesis allowing for random sampling of all possible mutant combinations. Mutants were expressed, purified, and tested in a semi-high throughput manner to select the ones with increased bundling activity as compared to wild-type PLS2. Several mutants were identified by sequencing, each harboring several mutations. One such mutant containing the fewest mutations (PLS2 WEL229/241/364CYP, designated as WEL/CYP hereafter) was further analyzed. All three mutations lie within the interior of the protein near the interface between ABD1 and ABD2 (Fig. 5a). We found that the WEL/CYP mutant is over 14 times more efficient at bundling actin than wild-type PLS2 (Fig. 5b, d). Intriguingly, WEL/CYP is also less stable than wild-type PLS2 with a melting temperature (T_m) similar to the individual ABDs (Fig. 4 and Fig. 5c), suggesting that the role of mutations is to release the inhibition from ABD1 on ABD2.

Actin releases ABD1-imposed inhibition of ABD2

We tested whether actin binding would be sufficient to release the inhibition of ABD2 by ABD1. To this end, we analyzed melting of plastin-actin mixtures by DSF. In order to reduce complexity and possible stabilization of ABD2 via interaction with actin as contributing factors to the outcome of these experiments, full-length PLS2 and phalloidin-stabilized actin filaments were mixed in the presence of Ca^{2+} to inhibit bundling and ensure that F-actin binding is only mediated through ABD1[27]. Upon binding to actin, PLS2 T_m significantly decreased to levels similar to the ones of individual ABDs and WEL/CYP mutant (Fig. 4 and Fig. 6a). This is consistent with the

results obtained using a PLS2 core construct (Fig. 4 and Fig. 6b), which has also been shown to be unable to bundle actin[30].

DISCUSSION

In this study, we describe a novel mechanism regulating the activity of human PLS2. Several studies have found that the two ABDs are not identical in their properties[23,26,28]. Importantly, we have previously shown that ABD1 is the primary actin-binding domain interacting with F-actin regardless of Ca^{2+} presence, whereas ABD2 is only activated under favorable conditions for actin bundle formation (e.g., when ABD1 is bound in low [Ca^{2+}]). Unexpectedly, here we have shown that ABD2 in separation binds F-actin with a much higher affinity than the full-length protein or ABD1. Furthermore, ABD2 is able to nucleate new actin filaments.

The lower-affinity ABD1 binding to F-actin prevailing over the higher-affinity ABD2 binding suggests that ABD2 is suppressed in the full-length PLS2 context[27]. Our data implies that this inhibition is imposed by ABD1. Indeed, ABD1 inhibits the ABD2-induced nucleation when added *in trans* by binding with a high affinity. In addition, the ABDs bind with low nanomolar affinity when combined *in trans*.

Bower and co-authors identified mutations in *S. cerevisiae* Sac6p that suppressed a mutant actin phenotype[29]. It was thought that these mutations are located on the actin-binding interface and their role in rescuing yeast is to increase association with actin. In light of new structural data obtained since this early study, we know that many of these residues are not surface-exposed and do not likely interact directly with actin. We reexamined these mutations and found that indeed they are able to significantly increase PLS2's ability to bundle F-actin. Since they are not likely to directly affect actin binding, we propose that they are disrupting the ABD1/ABD2 interaction and

increasing actin bundling by releasing ABD2 inhibition. This is supported by a decreased stability of this mutant to a level similar to the individual domains.

To form actin bundles, the inhibition of ABD2 must be released. Our data suggest that this release is achieved upon ABD1 binding to F-actin. Upon PLS2 binding to actin, its melting temperature is reduced to the levels observed for individual ABD1 and ABD2 domains, suggesting an actin-induced dissociation of the ABDs within the same protein, which would potentially release ABD2 inhibition and allow it to interact with actin. This hypothesis is supported by our previous finding that ABD1 is the primary ABD, binding under conditions when ABD2 does not. Such a mechanism, when the second domain obtains the ability to bind actin only after the first domain is bound to another filament may represent a 'zippering' mechanism of bundling wherein plastin molecules weakly bound via their ABD1 domains will dissociate from the filament unless the interaction is stabilized via ABD2 binding to another filament in proximity. Moreover, due to a helical nature of actin filaments, only productive interactions at the binding sites in the right register repeated every 36 nm will be favored, allowing the cell to retain plastin only in sites where actin bundling is needed.

Taken together these experiments suggest conservation of this regulation throughout evolution. Actin nucleation is not unique to human PLS2 as *S. pombe* Fim1 ABD2 but not full-length has been shown to nucleate filaments, albeit less efficiently[28]. Furthermore, the ability of PLS2 ABD2 to bind ABD1 from both PLS2 and PLS3 suggest that a similar interaction has been retained in each isoform. Finally, the mutations previously identified in *S. cerevisiae* are conserved in human PLS2 and likewise increase association with actin.

In summary, we have characterized a previously undescribed mode of PLS2 regulation wherein ABD1 is always available to bind F-actin but the high-affinity ABD2 is only able to bind

actin after ABD1 is bound. Future studies should investigate how this regulation is utilized within cells and determine the physiological relevance of actin nucleation by ABD2. This model also has implications in other modes of plastin regulation such as Ca^{2+}-binding and phosphorylation. It is possible that these modes of regulation are allosteric affecting the relationship between the ABDs rather than directly promoting or inhibiting interactions with actin.

METHODS

Protein expression and purification

Actin was purified from chicken skeletal muscle acetone powder [prepared in-house from flash-frozen chicken breasts (Trader Joe's)] as previously described[31]. Actin was stored up to one month on ice in G-buffer [5 mM Tris-HCl (pH 8.0), 0.2 mM $CaCl_2$, 0.2mM ATP, 5 mM β-mercaptoethanol (βME)] with dialysis against fresh G-buffer after two weeks. Plastin constructs were cloned into pColdI (Clontech) modified to include a TEV protease recognition site following the N-terminal 6xHis-tag. Proteins were expressed in BL21-CodonPlus(DE3)pLysS *Escherichia coli* (Agilent Technologies) grown in nutrient-rich media [1.25% tryptone, 2.5% yeast extract, 125 mM NaCl, 0.4% glycerol, 50 mM Tris-HCl (pH 8.2)]. Bacteria were grown to an OD_{600} of 1-1.2 before being cooled to 15 °C on ice. Expression was induced by addition of 1 mM IPTG and cells were grown at 15 °C for 15-20 hrs. Proteins were purified by immobilized metal affinity chromatography on Talon resin (Clontech). Purified proteins were dialyzed against PLS buffer [10 mM HEPES (pH 7.0), 30 mM KCl, 2 mM $MgCl_2$, 0.5 mM EGTA, 2 mM DTT, and 0.1 mM PMSF], flash-frozen in liquid nitrogen and stored at -80 °C.

Labeling proteins with fluorescent probes

Alexa 488-, and pyrene-labeled actins were prepared from G-actin in G-buffer devoid of reducing agents. Alexa 488-actin was prepared by labeling 2 mg/ml G-actin with 1.2 molar excess of Alexa Fluor 488-maleimide (ThermoFisher Scientific) for 4 h at 4^{o}C, followed by dilution to 1 mg/ml and polymerization with 2 mM $MgCl_2$ and 100 mM KCl overnight at 4^{o}C. Pyrene-actin was prepared by polymerizing 2 mg/ml G-actin with 2 mM $MgCl_2$ and 100 mM KCl at 25^{o}C for 30 min and then diluted to 1 mg/ml in F-buffer (5 mM Tris-HCl, pH 8, 0.2 mM ATP, 0.2 mM $CaCl_2$, 1 mM $MgCl_2$, 100 mM KCl). N-(1-pyrene)Iodoacetamide (ThermoFisher Scientific) was added to a final concentration of 40 µM and the labeling was carried out overnight with mixing at 4^{o}C. Both, Alexa 488 and pyrene labeling were quenched with 10 mM β-ME and labeled actins were pelleted at 45,000 rpm in Ti-70 (Beckman Courter) for 90 min followed by three rounds of dialysis of the resulted pellets against G-buffer. All labeled and unlabeled G-actins were further purified by size-exclusion chromatography on Sephacryl S200-HR (GE Healthcare), stored on ice in G-buffer and used within 4 weeks with a dialysis to G-buffer after two weeks of storage.

PLS2 ABD2 was labeled with fluorescein 5-maleimide (FM; ThermoFisher Scientific). Protein was incubated for 1 h on ice in the presence of 10 mM DTT. The reducing agent was removed by passing twice through a NAP5 desalting column (GE Healthcare) equilibrated with G-buffer lacking βME. Fluorescein was added at a 1.5-molar excess to protein and incubated overnight on ice. FM-ABD2 was passed through a NAP5 column equilibrated with G-buffer to remove excess dye.

Fluorescent anisotropy binding assays

G-actin was switched from Ca^{2+}- to Mg^{2+}-bound state by addition of 0.1 mM $MgCl_2$, and 0.5 mM EGTA and 10 min incubation on ice. Polymerization was induced by adding $MgCl_2$ to 2 mM, 30 mM KCl, and 10 mM HEPES (pH 7.0) and incubating for 30 min at room temperature.

F-actin was stabilized by a 1.2-molar excess of phalloidin. All reactions were carried out in PLS buffer supplemented with 0.2 mM ATP. For actin binding experiments, FM-ABD2 was used at 100 nM and F-actin was added at concentrations from 0 to 2500 nM. Reactions were incubated for 30 min at 25 °C prior to measurement. Parallel and perpendicular intensities were measured on an Infinite M1000 Pro plate reader (Tecan) with λ_{ex} = 470 nm and λ_{em} = 519 nm. Anisotropy was calculated:

$$Anisotropy = \frac{\| - \perp}{\| + (2\ \perp)}$$

Binding affinities were determined by fitting the data to the binding isotherm equation:

$$Fraction\ PLS\ Bound = \frac{P+A+K_d-\sqrt{(P+A+K_d)^2-4PA}}{2P},$$

where K_d is the dissociation constant, P is the concentration of plastin, and A is the concentration of F-actin.

Competition anisotropy experiments were carried out with 100 nM FM-ABD2 and 500 nM F-actin. Unlabeled ABD2 was added from 0 to 3000 nM. The dissociation constant of the unlabeled protein was determined by fitting the data to the following equation[32]:

$$Fraction\ FMABD2\ Bound =$$

$$\frac{-K_{d2}K_{d1}-2K_{d2}A-K_{d1}P+K_{d1}A+\sqrt{K_{d2}{}^2K_{d1}{}^2+2K_{d2}K_{d1}{}^2P+2K_{d2}K_{d1}{}^2A+K_{d1}{}^2P^2-2K_{d1}{}^2PA+K_{d1}{}^2A^2}}{2\left(K_{d2}K_{d1}-K_{d2}A-K_{d1}P+K_{d1}{}^2+K_{d1}A\right)},$$

where A is the concentration of F-actin, P is the concentration of ABD2, K_{d1} is the dissociation constant for FM-ABD2 binding to actin, and K_{d2} is the dissociation constant for unlabeled ABD2 binding to actin. Data fitting analysis was done using Origin software (OriginLab). Anisotropy experiments for ABD binding *in trans* were carried out similarly. The concentration of FM-ABD2 was 50 nM and ABD1 constructs were added at concentrations from 0 to 2500 nM. In the *trans*

ABD competition assays, FM-ABD2 was at 50 nM and ABD1 was kept at 250 nM. The concentration of unlabeled ABD2 varied from 0 to 5000 nM.

Actin bundling and binding co-sedimentation assays

In actin-binding experiments carried out in PLS buffer supplemented with 0.2 mM ATP, plastin constructs were used at a final concentration of 5 μM and F-actin (polymerized as above without the addition of phalloidin) was added from 0 to 50 μM. Actin-bundling experiments contained 2 μM F-actin and plastin concentrations from 0 to 1 μM. Reactions were incubated overnight at 4 °C followed by 1 h at room temperature. Binding reactions were spun at 300,000 g for 30 min at 25 °C using Optima MAX-TL ultracentrifuge (Beckman Coulter). Bundling reactions were spun at 17,000 g for 15 min at 25 °C. Supernatants and pellets were separated and analyzed by SDS-PAGE stained with Coomassie Brilliant Blue and quantified by densitometry using ImageJ software[33,34]. Dissociation constants were determined by fitting to the binding isotherm equation.

Bundling efficiency was quantified by fitting the data to the Hill equation:

$$\%\ Actin\ Bundled = \frac{[PLS]^n}{{K_A}^n + [PLS]^n},$$

where n is the Hill coefficient and ${K_A}^n$ is the concentration of plastin at 50% actin bundled.

Pyrenyl-actin polymerization assays

Ca^{2+}-ATP G-actin was added to a black 384-well plate (Corning) to a final concentration of 2.5 μM (5% pyrenyl-labeled). Next, Ca^{2+} was switched to Mg^{2+} by addition of 0.066 volumes of switch buffer [150 mM MOPS (pH 7.0), 3 mM ATP, 7.5 mM DTT, 4.5 mM EGTA, and 1.5 mM $MgCl_2$] and incubated for 1 min at room temperature. Polymerization was initiated by adding 0.33 volumes of initation buffer [30 mM MOPS (pH 7.0), 0.6 mM ATP, 1.5 mM DTT, 3 mM $MgCl_2$, and 90 mM KCl] as well as ABD2 to final concentrations from 0 – 2500 nM. In inhibition

experiments, ABD2 was maintained at 250 nM and ABD1 was added from 0 – 1000 nM. Pyrene fluorescence was monitored on an Infinite M1000 Pro plate reader (Tecan) with λ_{ex} = 365 nm and λ_{em} = 407 nm.

Total internal reflection fluorescence microscopy

For TIRF microscopy experiments, Ca^{2+}-ATP G-actin (final concentration 1.5 μM, 33% Alexa 488 labeled) was switched to Mg^{2+}-ATP G-actin by 2 min incubation in 0.05 mM $MgCl_2$ and 0.2 mM EGTA. Actin was mixed with or without 50 nM ABD2 in the final reaction buffer [10 mM imidazole (pH 7.0), 110 mM KCl, 50 mM DTT, 1 mM $MgCl_2$, 1 mM EGTA, 0.2 mM ATP, 0.05mM $CaCl_2$, 15 mM glucose, 20 μg/mL catalase, 100 μg/mL glucose oxidase, 3% glycerol, and 05% methylcellulose-400cP (Sigma Aldrich)]. Immediately upon mixing, reactions were transferred to an NEM-myosin treated flow chamber[35] and imaged using Nikon Eclipse Ti-E microscope equipped with a TIRF illumination module and a Perfect Focus System (Nikon).

Differential scanning fluorimetry

Temperature denaturation curves were obtained using a CFX Connect Real-Time PCR system (Bio-Rad). Reactions were carried out in PLS buffer supplemented with 0.2 mM ATP (when actin was present) and SYPRO Orange dye (1x final concentration; Invitrogen). Plastin constructs were added to a final concentration of 3 μM, while actin was added at 20 μM stabilized by phalloidin at 1.2-molar excess. Reactions containing ABD mixtures were incubated 30 min at 4 °C prior to measurement. Reactions containing actin were incubated overnight at 4 °C prior to measurement. The temperature was increased 2 °C per min with readings every 1 °C. Melting temperatures (T_m's) were determined by calculating the max of the first derivative of the fluorescence curve.

FIGURE LEGENDS

Figure 1. Actin-binding properties of individual PLS2 ABDs compared to the full-length protein.

(a-b) Binding of PLS2 (black squares) and PLS2 ABD1 (red circles) to F-actin was assayed by high-speed (300,000 g) co-sedimentation. PLS2 data were previously reported[27]. PLS2 FM-ABD2 (blue triangles) binding to F-actin was investigated using fluorescence anisotropy. (b) is a "blow-up" view of (a) in an actin concentration range from 0 to 2.5 μM. (c) Binding of F-actin by unlabeled ABD2 was determined using fluorescence anisotropy competition assays. (d) K_d values for (a-b) were determined by fitting the data to the binding isotherm equation. K_d values for (c) were calculated using the competition equation previously described[32]. Each data point is the average from three independent experiments. Error bars represent standard deviations.

Figure 2. Actin nucleation activity of PLS2 ABD2 is inhibited by ABD1.

(a) Bulk spontaneous assembly of pyrenyl-actin in the absence and presence of various concentrations of ABD2. Fluorescence is reported as % of maximum. (b) TIRF microscopy visualization of spontaneous Alexa 488-actin assembly in the presence and absence of 50 nM ABD2. (c) Inhibition of ABD2-induced actin nucleation by increasing concentrations of ABD1 *in trans*.

Figure 3. Interaction between PLS2 ABDs *in trans*.

(a, d, g, j) Binding between FM-ABD2 and various ABD1 constructs (PLS2 ABD1, PLS2 HpABD1, PLS3 ABD1, PLS3 HpABD1) was assessed by fluorescence anisotropy. (b, e, h, k) Binding between unlabeled ABD2 and ABD1 constructs was determined using fluorescence anisotropy competition experiments. Binding by HpABD1 constructs was investigated in the absence (black squares) and presence (open circles) of 1 mM Ca^{2+}. (c, f, i, l) Temperature-

dependent melting curves obtained by DSF in the presence of SYPRO Orange presented as the first derivative of the melting data. Curves were obtained for the individual ABDs (ABD1: black squares, ABD2: red circles) as well as for 1:1 mixture of the ABDs (blue triangles). Each data point is the average from three independent experiments. Error bars represent standard deviations. (m) K_d values for FM-ABD2 (a, d, g, j) were determined by fitting the data to the binding isotherm equation. K_d values for unlabeled ABD2 (b, e, h, k) were calculated using the competition equation[32].

Figure 4. PLS2 construct melting temperatures.

Melting temperatures of various PLS2 constructs individually as well as combined. T_ms were determined by calculating the maximum of the first derivative of the melting curves. Each data point is the average of three independent experiments. Error bars represent standard deviations. Statistical significance ($p < 0.005$) was determined using statistical hypothesis Student's *t* test and is indicated for relevant comparisons.

Figure 5. Properties of PLS2 WEL/CYP.

(a) Homology model of PLS2 core showing location of W229C, E241Y, and L364P (black spheres). (b) The bundling efficiency of wild-type PLS2 (black squares) and PLS2 WEL/CYP (open circles) was assessed using low speed (17,000 xg) co-sedimentation assays. (c) First derivative of thermal melting curves of wild-type PLS2 (black squares) and PLS2 WEL/CYP (red circles) monitored by DSF. Each data point is the average from three independent experiments. Error bars represent standard deviations. (d) Bundling efficiency, expressed as a concentration of PLS at 50% actin bundled, was quantified by fitting the data to the Hill equation.

Figure 6. Effect of F-actin on PLS2 stability.

Thermal melting curves of full-length (a) or a core (b) PLS2 (red circles), F-actin (black squares), and their mixtures (blue triangles) obtained by DSF. Presented curves are the first derivative of the data. Each data point is the average of three independent experiments. Error bars represent standard deviations.

REFERENCES

1 Pollard, T. D. & Cooper, J. A. Actin, a Central Player in Cell Shape and Movement. *Science* **326**, 1208-1212 (2009).

2 Pollard, T. D. & Borisy, G. G. Cellular Motility Driven by Assembly and Disassembly of Actin Filaments. *Cell* **112**, 453-465 (2003).

3 Schoenenberger, C. A., Mannherz, H. G. & Jockusch, B. M. Actin: from structural plasticity to functional diversity. *Eur J Cell Biol* **90**, 797-804, doi:10.1016/j.ejcb.2011.05.002 (2011).

4 Shinomiya, H. Plastin family of actin-bundling proteins: its functions in leukocytes, neurons, intestines, and cancer. *International journal of cell biology* **2012**, 213492, doi:10.1155/2012/213492 (2012).

5 Delanote, V., Vandekerckhove, J. & Gettemans, J. Plastins: versatile modulators of actin organization in (patho)physiological cellular processes. *Acta pharmacologica Sinica* **26**, 769-779, doi:10.1111/j.1745-7254.2005.00145.x (2005).

6 Grimm-Gunter, E. M. *et al.* Plastin 1 binds to keratin and is required for terminal web assembly in the intestinal epithelium. *Molecular biology of the cell* **20**, 2549-2562, doi:10.1091/mbc.E08-10-1030 (2009).

7 Lin, C. S., Shen, W., Chen, Z. P., Tu, Y. H. & Matsudaira, P. Identification of I-plastin, a human fimbrin isoform expressed in intestine and kidney. *Molecular and Cellular Biology* **14**, 2457-2467, doi:10.1128/mcb.14.4.2457 (1994).

8 Drenckhahan, D. *et al.* Three different actin filament assemblies occur in every hair cell: each contains a specific actin crosslinking protein. *Journal of Cell Biology* **112**, 641-651 (1991).

9 Sobin, A. & Flock, A. Immunohistochemical identification and localization of actin and fimbrin in vestibular hair cells in the normal guinea pig and in a strain of the waltzing guinea pig. *Acta Oto-Laryngologica* **96**, 407-412 (1983).

10 Jones, S. L., Wang, J., Turck, C. W. & Brown, E. J. A role for the actin-bundling protein L-plastin in the regulation of leukocyte integrin function. *Proceedings of the National Academy of Sciences of the United States of America* **95**, 9331-9336 (1998).

11 Ma, T., Sadashivaiah, K., Madayiputhiya, N. & Chellaiah, M. A. Regulation of sealing ring formation by L-plastin and cortactin in osteoclasts. *The Journal of biological chemistry* **285**, 29911-29924, doi:10.1074/jbc.M109.099697 (2010).

12 Morley, S. C. The actin-bundling protein L-plastin: a critical regulator of immune cell function. *International journal of cell biology* **2012**, 935173, doi:10.1155/2012/935173 (2012).

13 Morley, S. C. *et al.* The actin-bundling protein L-plastin dissociates CCR7 proximal signaling from CCR7-induced motility. *Journal of immunology* **184**, 3628-3638, doi:10.4049/jimmunol.0903851 (2010).

14 Todd, E. M., Deady, L. E. & Morley, S. C. The actin-bundling protein L-plastin is essential for marginal zone B cell development. *Journal of immunology* **187**, 3015-3025, doi:10.4049/jimmunol.1101033 (2011).

15 Wabnitz, G. H. *et al.* Costimulation induced phosphorylation of L-plastin facilitates surface transport of the T cell activation molecules CD69 and CD25. *European journal of immunology* **37**, 649-662, doi:10.1002/eji.200636320 (2007).

16 Wabnitz, G. H. *et al.* Sustained LFA-1 cluster formation in the immune synapse requires the combined activities of L-plastin and calmodulin. *European journal of immunology* **40**, 2437-2449, doi:10.1002/eji.201040345 (2010).

17 Lin, C. S., Park, T., Chen, Z. P. & Leavitt, J. Human Plastin Genes: comparative gene structure, chromosome location, and differenctial expression in normal and neoplastic cells. *The Journal of biological chemistry* **268**, 2781-2792 (1993).

18 Chaijan, S., Roytrakul, S., Mutirangura, A. & Leelawat, K. Matrigel induces L-plastin expression and promotes L-plastin-dependent invasion in human cholangiocarcinoma cells. *Oncology letters* **8**, 993-1000, doi:10.3892/ol.2014.2239 (2014).

19 Foran, E., McWilliam, P., Kelleher, D., Croke, D. T. & Long, A. The leukocyte protein L-plastin induces proliferation, invasion and loss of E-cadherin expression in colon cancer cells. *International journal of cancer. Journal international du cancer* **118**, 2098-2104, doi:10.1002/ijc.21593 (2006).

20 Klemke, M. *et al.* Phosphorylation of ectopically expressed L-plastin enhances invasiveness of human melanoma cells. *International journal of cancer. Journal international du cancer* **120**, 2590-2599, doi:10.1002/ijc.22589 (2007).

21 Riplinger, S. M. *et al.* Metastasis of prostate cancer and melanoma cells in a preclinical in vivo mouse model is enhanced by L-plastin expression and phosphorylation. *Molecular Cancer* **13** (2014).

22 de Arruda, M. V., Watson, S., Lin, C. S., Leavitt, J. & Matsudaira, P. Fimbrin Is a Homologue of the Cytoplasmic Phosphoprotein Plastin and Has Domains Homologous with Calmodulin and Actin Gelation Proteins. *The Journal of cell biology* **111**, 1069-1079 (1990).

23 Volkmann, N., DeRosier, D., Matsudaira, P. & Hanein, D. An Atomic Model of Actin Filaments Cross-linked by Fimbrin and Its Implications for Bundle Assembly and Function. *The Journal of cell biology* **153**, 947-956 (2001).

24 Lyon, A. N. *et al.* Calcium binding is essential for plastin 3 function in Smn-deficient motoneurons. *Human molecular genetics* **23**, 1990-2004, doi:10.1093/hmg/ddt595 (2014).

25 Namba, Y., Ito, M., Zu, Y., Shigesada, K. & Maruyama, K. Human T Cell L-Plastin Bundles Actin Filaments in a Calcium Dependent Manner. *Journal of Biochemistry* **112**, 503-507 (1992).

26 Galkin, V. E., Orlova, A., Cherepanova, O., Lebart, M. C. & Egelman, E. H. High-resolution cryo-EM structure of the F-actin-fimbrin/plastin ABD2 complex. *Proceedings of the National Academy of Sciences of the United States of America* **105**, 1494-1498, doi:10.1073/pnas.0708667105 (2008).

27 Schwebach, C. L., Agrawal, R., Lindert, S., Kudryashova, E. & Kudryashov, D. S. The Roles of Actin-Binding Domains 1 and 2 in the Calcium-Dependent Regulation of Actin Filament Bundling by Human Plastins. *Journal of molecular biology*, doi:10.1016/j.jmb.2017.06.021 (2017).

28 Skau, C. T. *et al.* Actin filament bundling by fimbrin is important for endocytosis, cytokinesis, and polarization in fission yeast. *The Journal of biological chemistry* **286**, 26964-26977, doi:10.1074/jbc.M111.239004 (2011).

29 Brower, S. M., Honts, J. E. & Adams, A. E. Genetic Analysis of the Fimbrin-Actin Binding Interaction in Saccharomyces cerevisiae. *Genetics* **140**, 91-101 (1995).

30 Ishida, H., Jensen, K. V., Woodman, A. G., Hyndman, M. E. & Vogel, H. J. The Calcium-Dependent Switch Helix of L-Plastin Regulates Actin Bundling. *Scientific reports* **7**, 40662, doi:10.1038/srep40662 (2017).

31 Spudich, J. A. & Watt, S. The Regulation of Rabbit Skeletal Muscle Contraction. *The Journal of biological chemistry* **246**, 4866-4871 (1971).

32 Nolen, B. J. & Pollard, T. D. Structure and biochemical properties of fission yeast Arp2/3 complex lacking the Arp2 subunit. *The Journal of biological chemistry* **283**, 26490-26498, doi:10.1074/jbc.M802607200 (2008).

33 Schindelin, J. *et al.* Fiji: an open-source platform for biological-image analysis. *Nat Methods* **9**, 676-682, doi:10.1038/nmeth.2019 (2012).

34 Schindelin, J., Rueden, C. T., Hiner, M. C. & Eliceiri, K. W. The ImageJ ecosystem: An open platform for biomedical image analysis. *Mol Reprod Dev* **82**, 518-529, doi:10.1002/mrd.22489 (2015).

35 Kovar, D. R. & Pollard, T. D. Insertional assembly of actin filament barbed ends in association with formins produces piconewton forces. *Proceedings of the National Academy of Sciences of the United States of America* **101**, 14725-14730, doi:10.1073/pnas.0405902101 (2004).

FIGURES

Figure 1

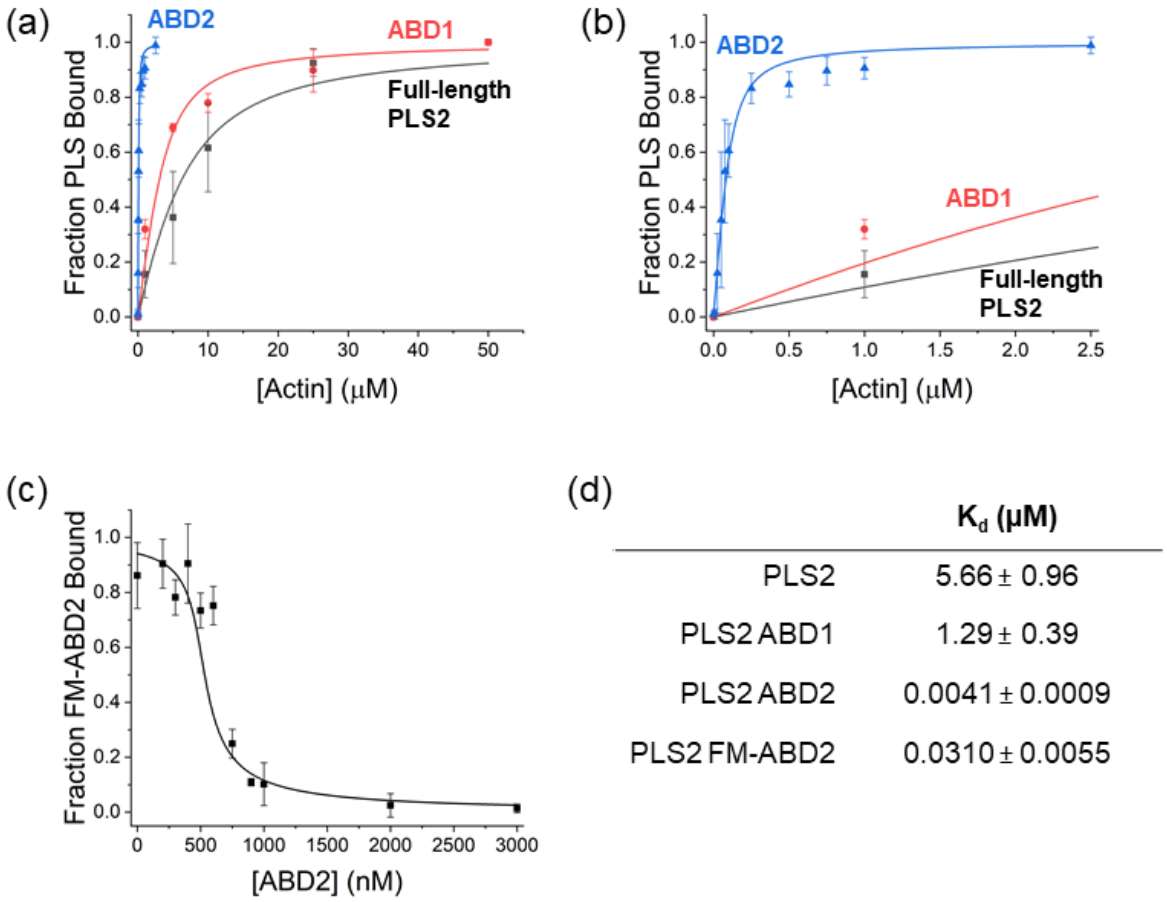

(d)

	K_d (μM)
PLS2	5.66 ± 0.96
PLS2 ABD1	1.29 ± 0.39
PLS2 ABD2	0.0041 ± 0.0009
PLS2 FM-ABD2	0.0310 ± 0.0055

Figure 2

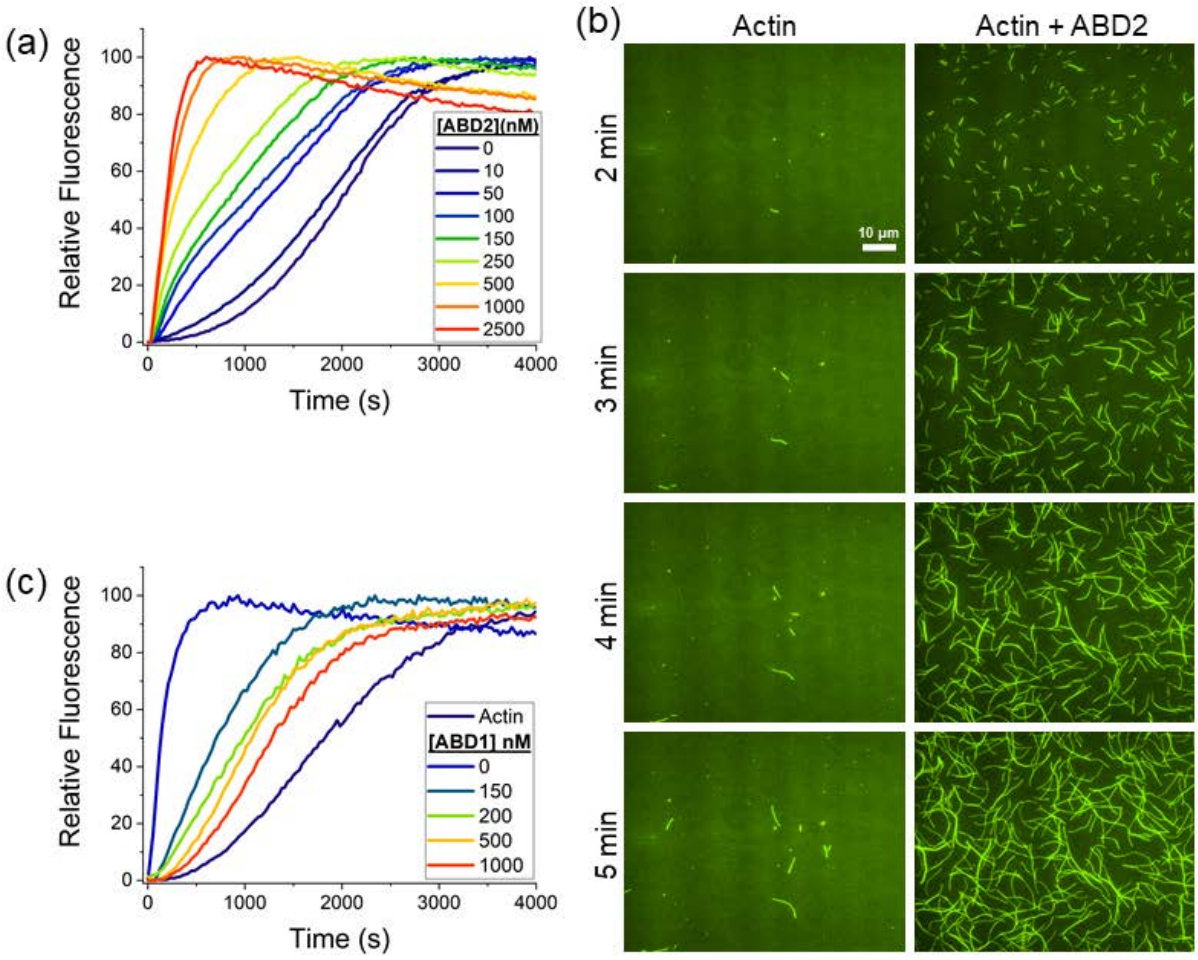
(a)
Relative Fluorescence
Time (s)
[ABD2](nM)
0
10
50
100
150
250
500
1000
2500
(b)
Actin
Actin + ABD2
2 min
3 min
4 min
5 min
10 µm
(c)
Relative Fluorescence
Time (s)
Actin
[ABD1] nM
0
150
200
500
1000

Figure 3

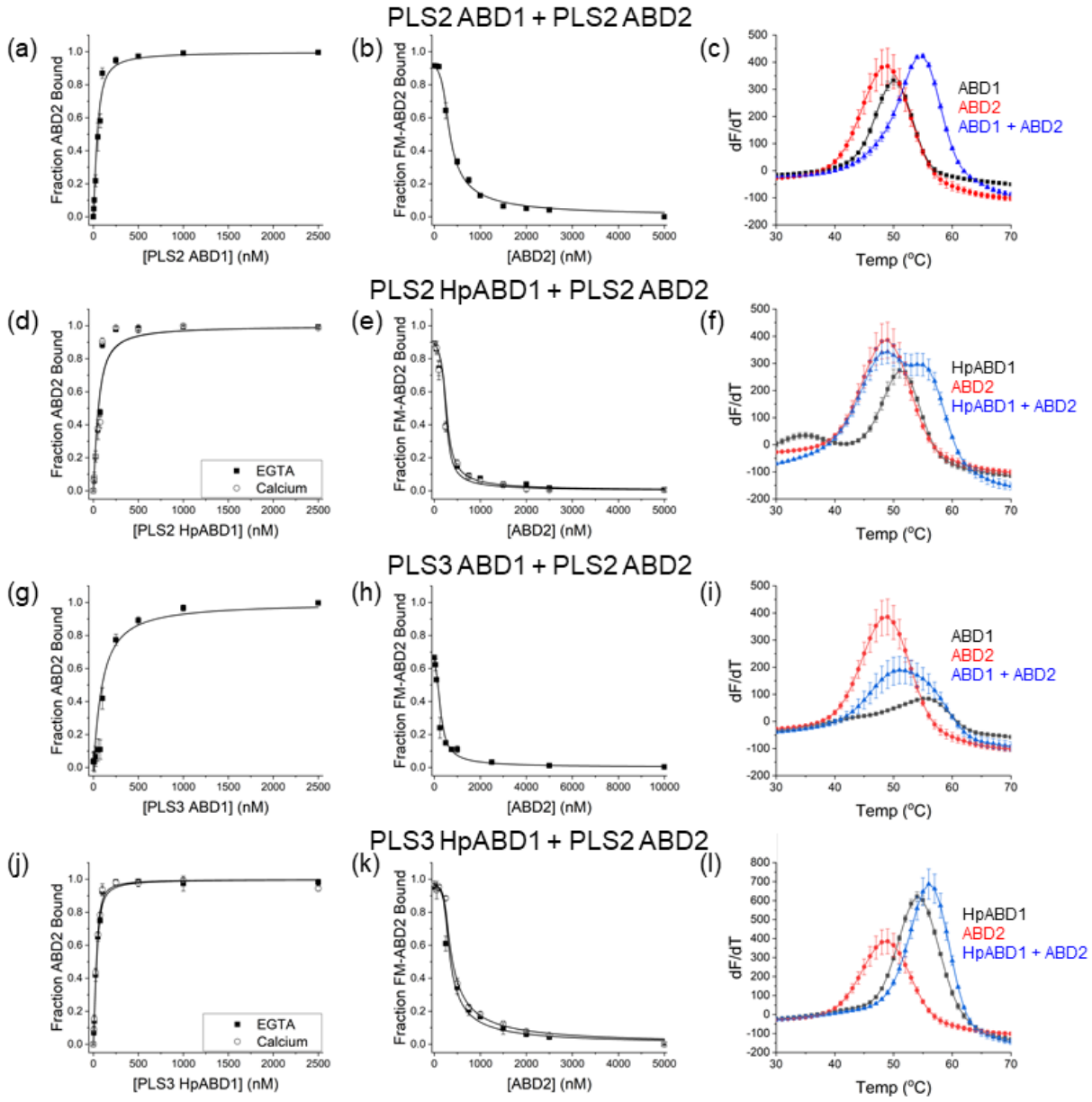

(m)

	FM-ABD2 K_d (nM)	ABD2 K_d (nM)
PLS2 ABD1	20.53 ± 2.17	11.43 ± 0.74
PLS2 HpABD1 – EGTA	29.83 ± 3.77	3.01 ± 0.92
PLS2 HpABD1 – Ca^{2+}	30.75 ± 3.28	2.94 ± 0.48
PLS3 ABD1	131.65 ± 12.76	19.17 ± 8.74
PLS3 HpABD1 – EGTA	8.65 ± 1.27	4.24 ± 0.67
PLS3 HpABD1 – Ca^{2+}	7.30 ± 0.38	4.65 ± 0.30

Figure 4

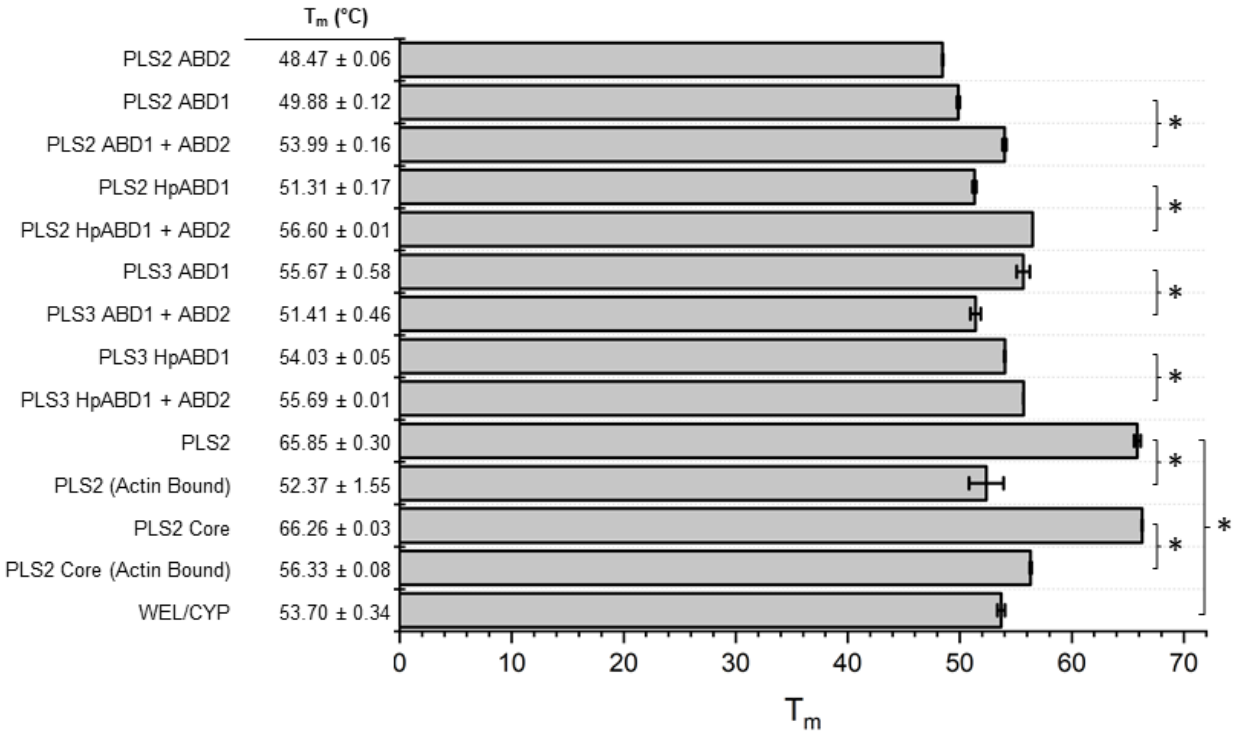
T_m (°C)
PLS2 ABD2
48.47 ± 0.06
PLS2 ABD1
49.88 ± 0.12
PLS2 ABD1 + ABD2
53.99 ± 0.16
PLS2 HpABD1
51.31 ± 0.17
PLS2 HpABD1 + ABD2
56.60 ± 0.01
PLS3 ABD1
55.67 ± 0.58
PLS3 ABD1 + ABD2
51.41 ± 0.46
PLS3 HpABD1
54.03 ± 0.05
PLS3 HpABD1 + ABD2
55.69 ± 0.01
PLS2
65.85 ± 0.30
PLS2 (Actin Bound)
52.37 ± 1.55
PLS2 Core
66.26 ± 0.03
PLS2 Core (Actin Bound)
56.33 ± 0.08
WEL/CYP
53.70 ± 0.34
*
*
*
*
*
*
*
0
10
20
30
40
50
60
70
T_m

Figure 5

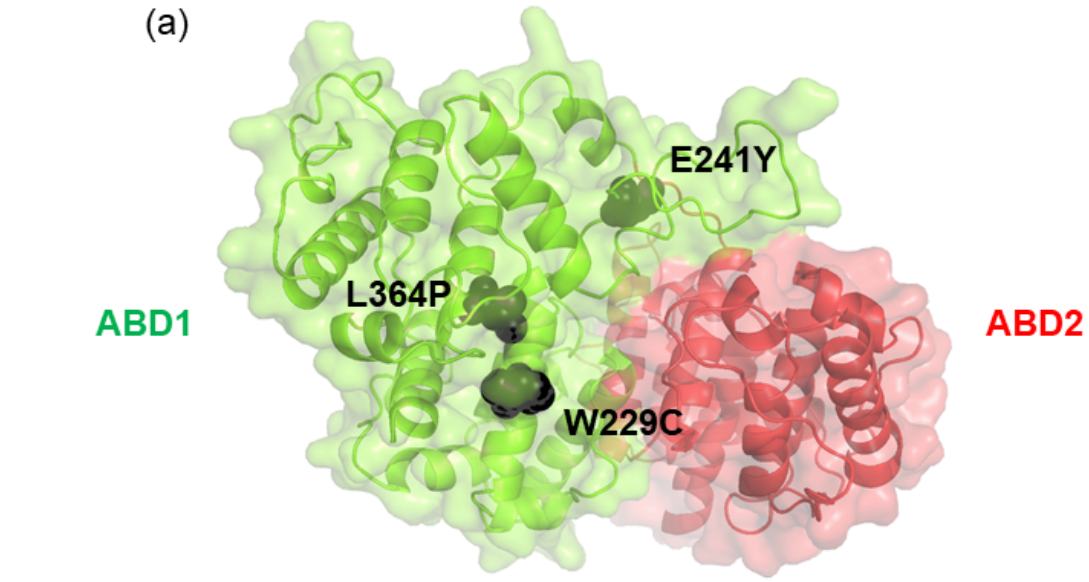

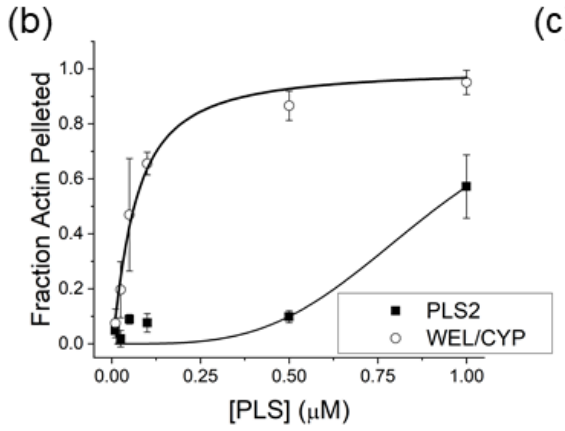

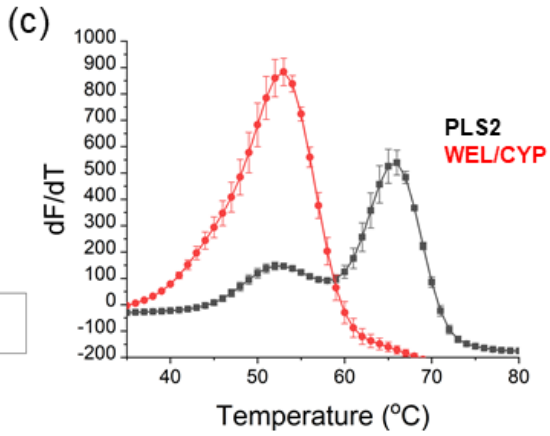

(d)

	WEL/CYP	PLS2
[PLS] (μM) at 50% Bundled Actin	0.063 ± 0.006	0.923 ± 0.063

Figure 6

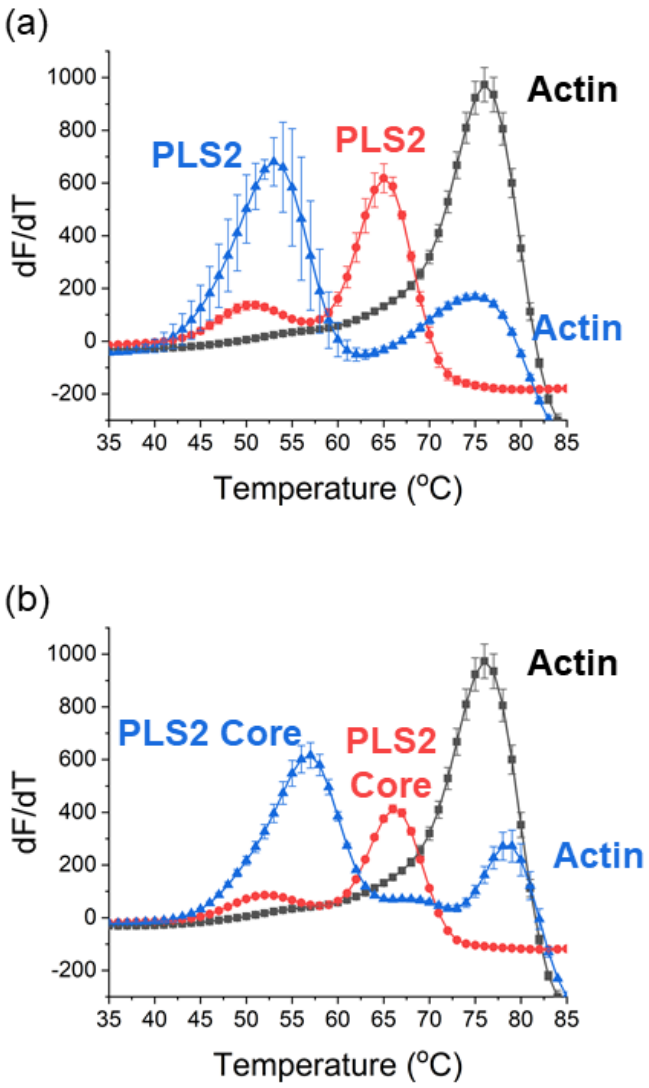
(a)
1000
800
600
400
200
0
-200
dF/dT
PLS2
PLS2
Actin
Actin
35 40 45 50 55 60 65 70 75 80 85
Temperature (°C)
(b)
1000
800
600
400
200
0
-200
dF/dT
PLS2 Core
PLS2
Core
Actin
Actin
35 40 45 50 55 60 65 70 75 80 85
Temperature (°C)